ACS OMEGA

http://pubs.acs.org/journal/acsodf

Article

Memantine-Derived Schiff Bases as Transdermal Prodrug Candidates

Ana P. Araujo de Oliveira, Victoria C. Romero Colmenares, Renata Diniz, Jennifer T. J. Freitas, Clara M. da Cruz, Eduardo B. Lages, Lucas A. M. Ferreira, Rafael P. Vieira,* and Heloisa Beraldo*

Cite This: *ACS Omega* 2022, 7, 11678−11687

Read Online

ACCESS | Metrics & More | Article Recommendations | Supporting Information

ABSTRACT: Condensation reactions of salicylaldehyde, 2-pyridinecarboxaldehyde, and pyridoxaldehyde with memantine (**Me**) produced novel memantine-derived Schiff bases (**1**−**3**). Speciation predictions and calculations of Log P, Log D, and of the percentage (%) of neutral species for (**1**−**3**) were carried out. In comparison with **Me**, the Schiff bases presented increased log P and log D in all cases and pH values, suggesting higher hydrophobicity. The determined solubilities in *n*-octanol were 34.7 mg/mL for memantine hydrochloride and 67.3 mg/mL for (**3**). According to the molecular weights and calculated logP, compounds (**1**−**3**) are suitable for transdermal administration, especially compound (**3**). In addition, hydrolysis of **3** with the release of pyridoxal, a daily cofactor in human metabolism, was observed. The results suggested that **3** is the most promising compound and that formation of the pyridoxal Schiff base with **Me** might be an effective strategy to obtain a prodrug candidate with increased lipophilicity, which would be able to passively cross biological barriers during transdermal delivery and might have applications in the treatment of Alzheimer's disease and other neurological disorders.

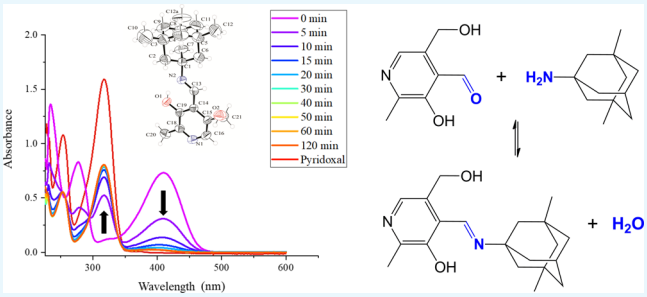

INTRODUCTION

Neurodegenerative diseases are often characterized by progressive impairment of central nervous system functions, such as cognitive and motor abilities. These pathological conditions directly affect social and occupational skills, contributing to the physical and emotional stress of patients, families, and professionals. Around 50 million patients worldwide suffer from dementia, mainly adults aged 85 years old and over, and that number is expected to triple by 2050, as a result of the increase in life expectancy worldwide.[1] Alzheimer's disease (AD) is the most common type of dementia, representing up to 60−70% of all cases.[1] AD is characterized by several biochemical hallmarks, including protein misfolding,[2,3] oxidative stress, and metal ions imbalance.[4−6] Despite all the recent efforts on the characterization of AD pathophysiological processes, the cause of the disease is not well understood.

Currently, three acetylcholinesterase inhibitors and memantine are used in the treatment of AD, but they are only able to alleviate symptoms of dementia and not to halt the evolution of the degenerative process.[7] Aducanumab was approved by the US Food and Drug Administration (FDA) in June 2021 for the treatment of AD based on its capacity to reduce the levels of β-amyloid plaques in the brain, a possible cause of the disease. However, data did not conclusively show that aducanumab could slow cognitive decline.[8]

N-methyl-D-aspartate (NMDA) receptors (NMDARs) are ionotropic glutamate receptors mainly involved in synaptic plasticity inherent to memory and learning. However, they are also major actors of excitotoxic harm that occurs during chronic neurodegenerative disorders. Synaptic NMDAR (sNMDAR) contributes to cell plasticity and neurotrophic processes, whereas extrasynaptic NMDAR (eNMDAR) triggers apoptotic signaling processes. Selective targeting of the eNMDARs constitutes a promising strategy to treat neurodegenerative conditions.[9]

Memantine (3,5-dimethyladamantan-1-amine, **Me**, Figure 1A) is an uncompetitive NMDAR antagonist approved in the United States to treat moderate−severe AD patients.[7] Its mode of action involves an open-channel blockage with a relatively fast off-rate from the channel. Hence, memantine mainly enters the channel in conditions of extreme and prolonged glutamate exposure, acting on extrasynaptic/tonically activated over synaptic/phasically activated NMDAR. This distinctive profile allows memantine to contrast excitotoxicity while keeping

Received: November 21, 2021
Accepted: March 16, 2022
Published: March 28, 2022

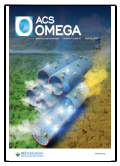

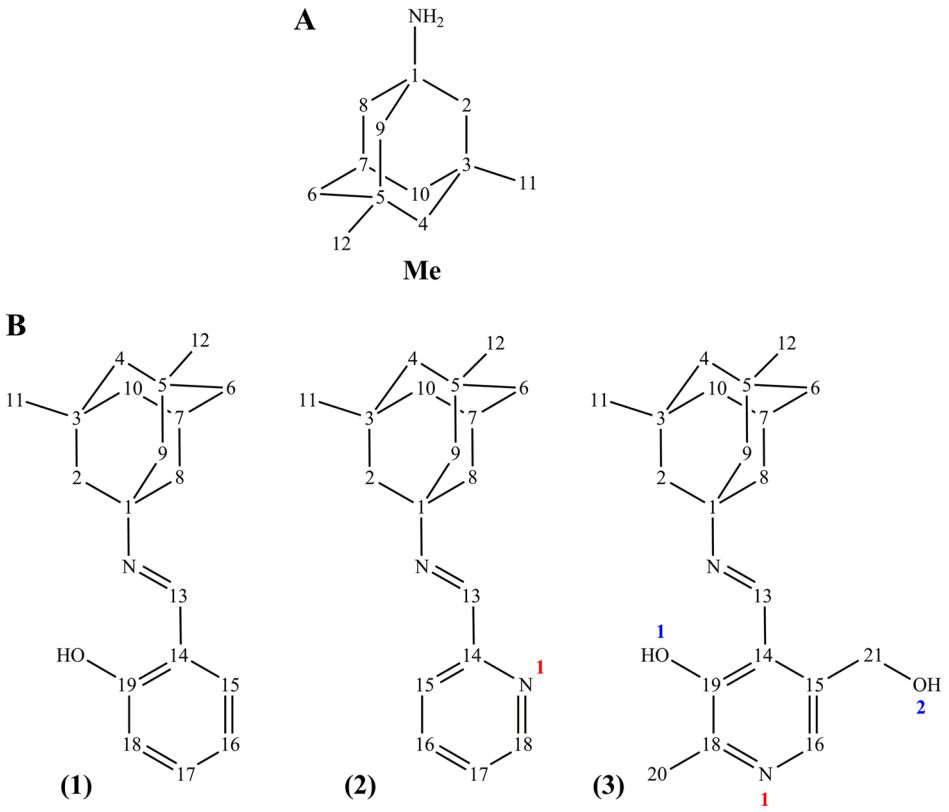

Figure 1. Structural representations of memantine (**Me**, **A**) and its Schiff base derivatives (**1**, **2**, and **3** (**PyMe**), **B**).

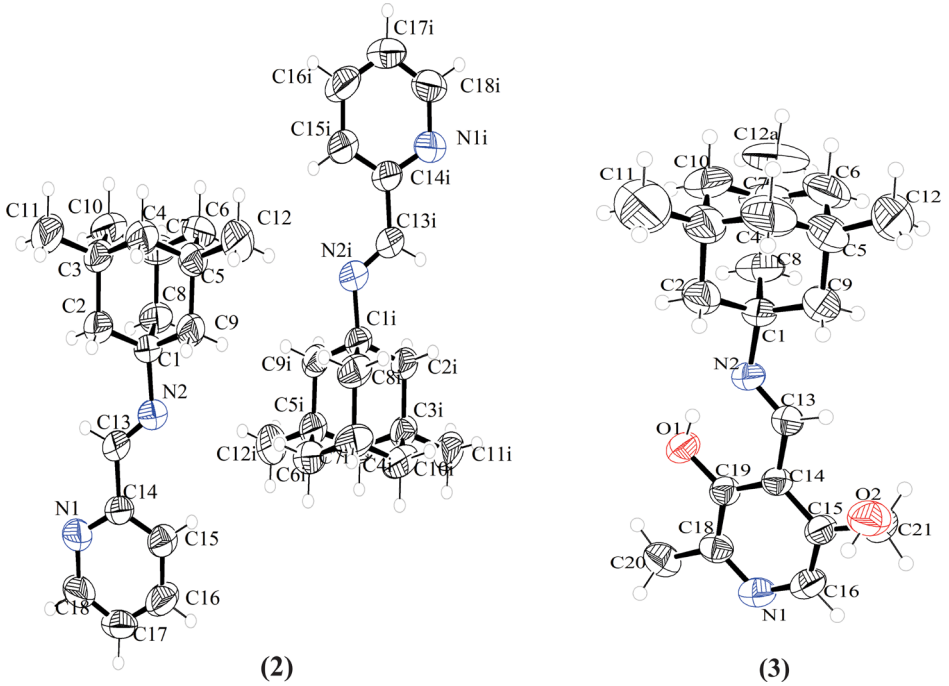

Figure 2. Molecular plots of **2** and **3** showing the labeling of the non-H atoms and their displacement ellipsoids at the 50% probability level.

glutamatergic synaptic functioning, which probably accounts for its clinical tolerability.[9]

Since the molecule-based development of new tools aiming at AD pharmacotherapy is still challenging, the improvement of the current treatments centered on standard drugs is of paramount importance.

In many of the stages in which **Me** tablets are employed, patients present swallowing disorders and significant changes in behavior, risking adherence to pharmacotherapy.[10,11] Therefore, providing the administration by new, safe, and effective ways represents a promising tool to ensure a suitable treatment. Drugs used for the treatment of AD, including **Me** in its unaltered form, have already been evaluated in the

https://doi.org/10.1021/acsomega.1c06571
ACS Omega 2022, 7, 11678−11687

Table 1. Crystal Data and Refinement Results for Compounds (2) and (3)

compound	2	3
empirical formula	$C_{18}H_{24}N_2$	$C_{20}H_{28}N_2O_2$
formula weight ($g{\cdot}mol^{-1}$)	268.40	328.45
crystal system	Monoclinic	Triclinic
space group	$P2_1/c$	$P\bar{1}$
wavelength (λ)	0.71073	0.71073
temperature (K)	293(2)	293(2)
a (Å)	11.7565(5)	7.9246(7)
b (Å)	15.4536(7)	8.0230(6)
c (Å)	18.0466(9)	16.8042(13)
$\alpha/\beta/\gamma$ (°)	90.0/105.446(5)/90.0	92.659(6)/98.121(7)/116.757(8)
volume ($Å^3$)	3160.3(3)	937.09(14)
Z	8	2
density calculated ($mg{\cdot}cm^{-3}$)	1.128	1.160
$F(000)$	1168	354
absorption coefficient (mm^{-1})	0.066	0.075
limiting indices	$-15 \le h \le 16$	$-10 \le h \le 10$
	$-20 \le k \le 20$	$-10 \le k \le 10$
	$-23 \le l \le 24$	$-23 \le l \le 23$
θ range for data collection (°)	2.284 to 29.524	2.468 to 29.548
reflections collected	50906	12419
independent reflections [R_{int}]	0.0913	0.0357
completeness to θ = 29.562 (%)	99	100
data/restraints/parameters	8191/0/365	4506/0/228
final R indices [$I > 2\sigma(I)$]	R_1 = 0.0664 wR_2 = 0.1725	R_1 = 0.0631 wR_2 = 0.1658
R indices (all data)	R_1 = 0.1486 wR_2 = 0.2253	R_1 = 0.1228 wR_2 = 0.2062
goodness-of-fit on F^2	1.019	1.028
$\Delta\rho_{max.}$ e $\Delta\rho_{min.}$	0.167, −0.162	0.204, −0.187

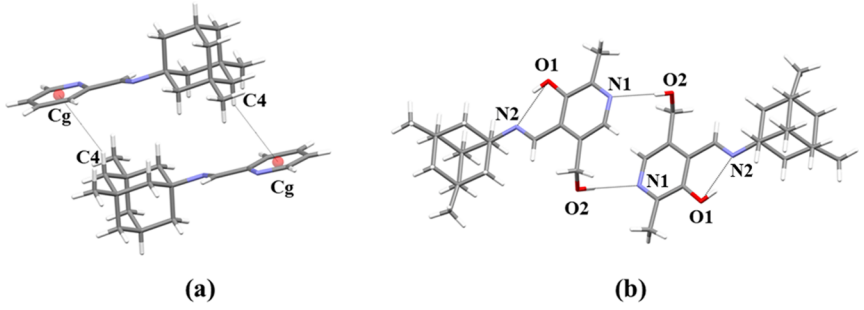

Figure 3. Intermolecular interactions in (a) compound (2) and (b) compound (3).

context of transdermal administration, which is effective for patient adherence to the treatment and consequent burden relief of caregivers.[12−14]

In previous studies we investigated Schiff bases with potential applications in the treatment of AD.[15,16] In the present work, novel memantine-derived Schiff bases (**1**, **2**, and **3**, Figure 1) were synthesized by reacting pyridoxaldehyde, salicylaldehyde, and 2-pyridinecarboxaldehyde with memantine hydrochloride. Since pyridoxaldehyde (**Py**) is one of the forms of vitamin B6, the **PyMe** conjugate (**3**) was investigated as a promising prodrug candidate for transdermal **Me** release, with the possible ability to improve the currently established AD pharmacotherapy.

RESULTS AND DISCUSSION

IR and NMR Characterization. The signal of NH_2 is observed at 8.12 ppm in the ^{1}H NMR spectrum of **Me**. This signal is absent in the spectra of **1**, **2**, and **3**. Signals of the aromatic hydrogens of salicylaldehyde are observed at 6.89−7.46 ppm in the spectrum of **1**, and those of 2-pyridinecarboxaldehyde are found at 7.39−7.93 ppm in the spectrum of **2**. In the ^{13}C and HMQC NMR spectra of **1**−**3**, the signals of the aromatic carbons and the signal of the azomethine carbon C13 are observed along with those of 3,5-dimethyladamantane, in agreement with the formation of the Schiff base compounds (see Figures S1−S14, Supporting Information).

The absorptions attributed to the $\upsilon(NH_2)$ stretching are observed at 3412−2746 cm^{-1} in the infrared spectrum of **Me**. As expected, these vibrational modes are absent in the spectra of **1**, **2**, and **3**. The absorptions attributed to $\upsilon(C{=}N)$ were found at 1627, 1644, and 1632 cm^{-1} in the spectra of **1**, **2**, and **3**, respectively, confirming the formation of the Schiff bases (see Figures S15−S17, Supporting Information).

Crystal Structures of 2 and 3. Figure 2 shows the atom arrangements and numbering scheme for **2** and **3**. Compound (**2**) crystallized in the monoclinic system $P2_1/c$ space group, with two molecules per asymmetric unit, while compound (**3**)

https://doi.org/10.1021/acsomega.1c06571
ACS Omega 2022, 7, 11678−11687

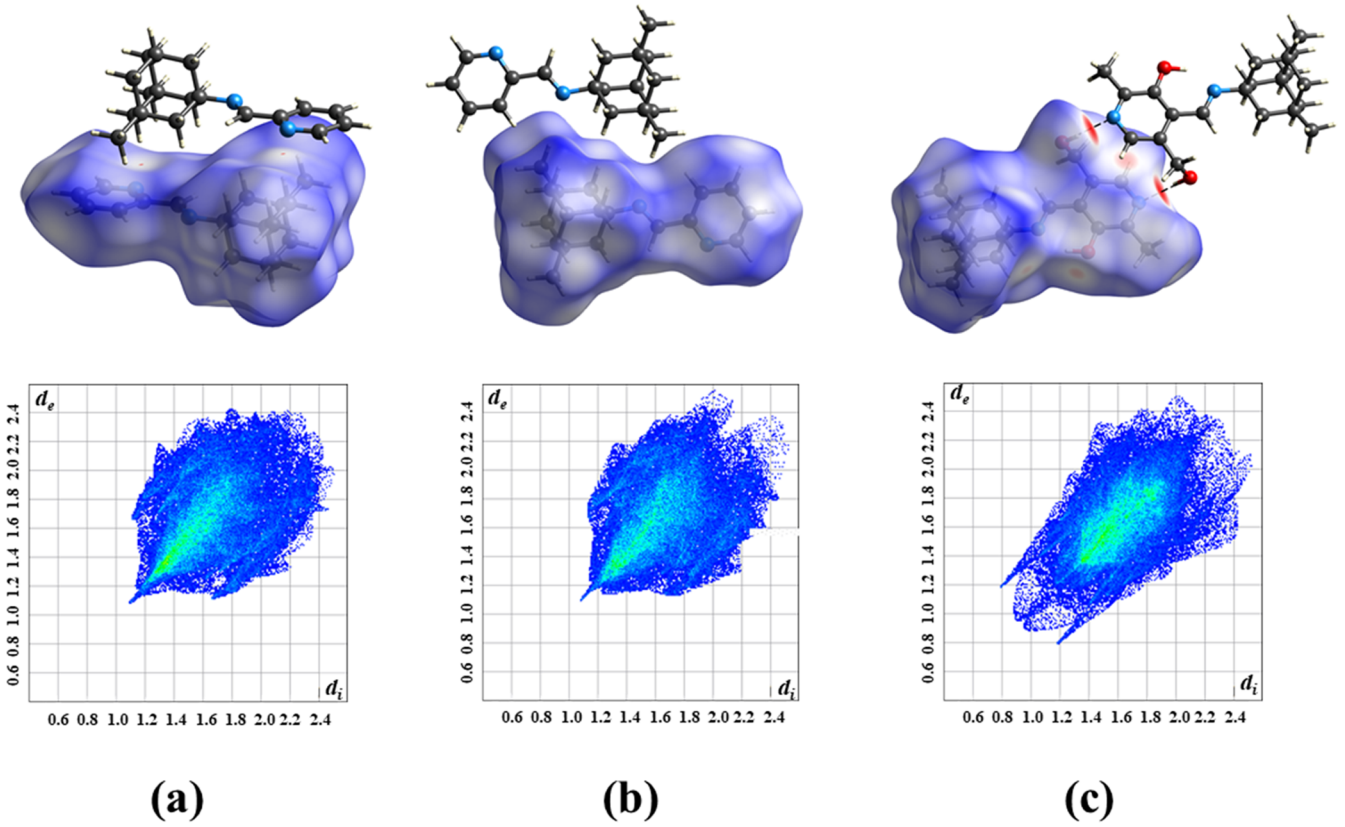

Figure 4. Hirshfeld surface and fingerprint plots for compound (**2**) (**a**) molecule A, (b) molecule B, and (c) compound (**3**).

crystallized in the $P\bar{1}$ triclinic space group. Table 1 reports crystal data and refinement results, and Table S1 (Supporting Information) reports selected bond distances and angles for both compounds. The C(13)-N2 distances are1.226(2) and 1.233(2) Å (compound 2), and 1.265(2) Å (compound 3), which is comparable to C═N bond distances in similar compounds (average of 1.27(2) Å, using 243 structures in the MOGUL program).[17] The torsion angle between the aromatic ring and the plane formed by C2, C8, and C9 atoms for both molecules of compound (**2**) is similar (82.3 and 84.2°). This torsion angle (C2, C8, and C9 plane with the aromatic ring) in compound (**3**) is a little bigger (89.0°), suggesting that substitution in the aromatic ring promotes a small modification in the molecular conformation.

In compound (**2**) the independent molecules (A and B) and the A molecules interact with each other by CH···π interactions, giving rise to a dimeric arrangement (distance C4···Cg = 3.98 Å, where Cg is the centroid of the aromatic ring), as illustrated in Figure 3a. These interactions are displayed in the Hirshfeld surface[18] as small red points (Figure 4a), which are not observed in molecule B (Figure 4b). The volume and area of the surface are similar for molecule A (388.85 Å^3 and 330.50 Å^2, respectively) and molecule B (388.00 Å^3 and 327.95 Å^2, respectively), being slightly bigger in A. For B molecules, only H···H interactions were observed. The fingerprint plots[19] indicate that H···H and C···H interactions are responsible for the crystal stability of compound (**2**), representing an average of 76 and 15%, respectively, for molecules A and B (Figure 4a,b). The graphs are similar for molecules A and B, but molecule B presents higher values of d_i and d_e and more dispersed dots than molecule A. These dots are related to long-distance H···H interactions and suggest that for B there is more empty space around the molecules in comparison to A.[19]

On the other hand, compound (**3**) presents stronger intermolecular interactions due to the presence of OH groups (Figure 2), which form intra and intermolecular OH···N hydrogen bonds, with O2···N1 distance of 2.879(3) Å and intramolecular interactions with O1···N2 distance of 2.581(2) Å. The intermolecular interactions give rise to a dimeric arrangement in the solid state (Figure 3b).

In the fingerprint plots of compound (**3**) (Figure 4c), as in compound 2, the most frequent interactions are H···H, representing 76% in the crystal structure, whereas the N···H and O···H interactions represent 5.4 and 9.1%, respectively.

Comparing the fingerprint plots of compounds (**2**) and (**3**), the main difference occurs due to the sharp features related to N−H···O hydrogen bonds, the H···H interactions being more diffuse in compound (**3**). The small distance (di + de) for this interaction is around 1.9 Å in compound (**3**) and 2.2 Å in compound (**2**), indicating that the crystal packing in compound (**3**) is more compact than in compound (**2**).

Calculated and Experimental Physicochemical Properties. In the present study we intended to evaluate different physicochemical properties of compounds (**1**−**3**) in comparison to those of the parent primary amine, **Me**. Hence, speciation predictions were performed for compounds (**1**−**3**). The species and speciation diagrams for compounds (**1**) and (**2**) are in Figures S21 and S22 (Supporting Information), and those of compound (**3**) are presented in Figure 5. Table 2 contains the percentage of neutral species for the compounds at pH = 5, pH = 5.5, and pH = 7.4.

The predicted speciation diagram for **3** (Figure 5) suggests that this compound would be suitable for transdermal delivery

https://doi.org/10.1021/acsomega.1c06571
ACS Omega 2022, 7, 11678−11687

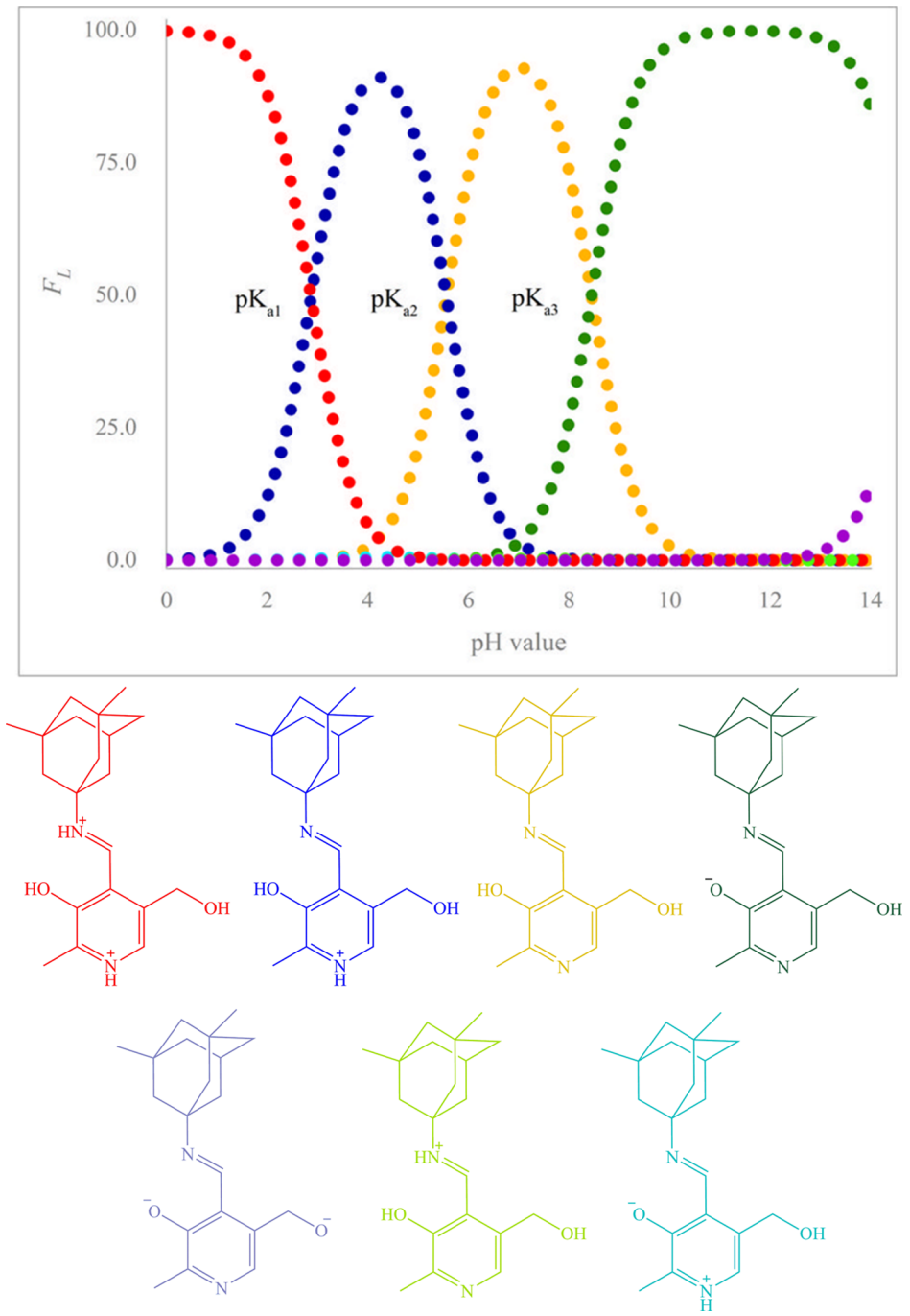

Figure 5. Speciation diagram of compound (**3**). F_L = fraction of species. Diagram was predicted using https://chemicalize.com/(http://www.chemaxon.com).[20]

Table 2. Theoretical Values of Log P, Log D, and the Percentage (%) of Neutral Species for Me, 1, 2, and 3[a]

		log D			neutral species (%)		
		pH values			pH values		
compound	log P	5.0	5.5	7.4	5.0	5.5	7.4
Me	2.07	−0.97	−0.96	−0.78	0	0	0
1	4.31	3.31	3.73	4.28	10	26	93
2	4.07	4.06	4.07	4.07	97	99	100
3	2.46	1.84	2.14	2.41	21	46	90

[a]The LogD values and percentage of neutral species were calculated at pH values of 5.0, 5.5, and 7.4.[20,21]

since a considerable amount (21−46%) of the neutral species of **3** is present in the 5.0−5.5 pH range. This neutral species would be able to better passively cross biological barriers in comparison to its ionized forms.

The fulfillment of basic structural and physicochemical properties, such as appropriate lipophilicity, a maximum molecular weight of 500 g.mol^{-1}, and a melting point lower than 250 °C by compounds targeting passive transdermal delivery, is desirable.[22−24] Appropriate lipophilicity can be quantitatively understood as molecules presenting log P values between 1 and 3,[22,23,25] or even lower than 5.[24]

The calculated LogP and LogD values for **Me**, **1**, **2**, and **3** are shown in Table 2. In comparison with **Me**, the Schiff bases

https://doi.org/10.1021/acsomega.1c06571
ACS Omega 2022, 7, 11678−11687

present increased logP and logD in all cases and pH values, suggesting higher hydrophobicity for the three aldimines.

In addition, according to the molecular weights and calculated logP values displayed in Table 2, compounds (**1**−**3**) could be suitable for transdermal administration. Especially considering logP values between **1** and **3**, compound (**3**) might be suggested as the most promising prodrug candidate among the three compounds. Furthermore, increased hydrophobicity of prodrug candidates, such as in compound (**3**), is a gain of function in terms of passive transdermal delivery.

The solubility values (mg/mL) of memantine hydrochloride and **3** in *n*-octanol were determined as a first indicator on the evaluation of their distribution in aqueous media, such as serum, and simultaneous ability to cross biological barriers, such as cell membranes and the skin. According to Figure 6,

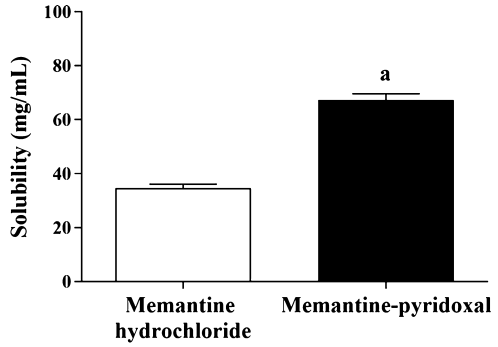

Figure 6. Solubility of memantine hydrochloride and the memantine−pyridoxal conjugate compound (**3**). Error bars represent variation between three replicates. Unpaired *t*-test was applied and "a" represents a statistically significant difference ($p < 0.0001$) between memantine hydrochloride and memantine-pyridoxal.

the solubility value of memantine hydrochloride in *n*-octanol was 34.7 mg/mL, while the solubility of compound **3** was 67.3 mg/mL, 1.9-fold higher. These values suggest the formation of a Schiff base between **Py** and **Me**, forming **3**, as an effective strategy to obtain a potential prodrug with increased lipophilicity. These results are in accordance with the higher log P and log D values predicted for **3**, in comparison to the same parameters for **Me**, as shown in Table 2.

Schiff bases are compounds presenting imine bonds (C═N), which are obtained from condensation reactions between primary amines and carbonyl compounds−aldimines, if originated from aldehydes, and ketimines, if obtained from ketones.[26−28] One of the most important characteristics of Schiff bases is their susceptibility to nucleophilic attack,[29,30] especially in acidic conditions,[31,32] leading to the imine bond breakdown and consequently yielding the original reagents. This liability may be related to the groups linked to the C═N bond and, despite being just a drawback regarding stability, it is also a necessary feature, considering reversibility in the context of several crucial metabolic reactions. One of the classic examples is vitamin B6 and associated enzymes. Pyridoxal-5′-phosphate (PLP), one of the B6 vitamers,[33] reacts with side chains of lysine residues in specific enzymes and forms transient Schiff bases, acting as an essential cofactor.[34] Important amino acid transamination reactions,[35−37] neurotransmitter formation,[38,39] and drugs biotransformation[40,41] are strictly dependent of this specific and reversible C═N bond formation between PLP and its related enzymes.

Hence, we also investigated the liability of **3** in an aqueous solution at different pH values, simulating human organism conditions to which the compound could be exposed considering a transdermal administration.

Time-dependent UV−vis absorption spectra were obtained for compound (**3**) at pH 5.0 and 7.4, simulating the skin surface (range of pH 4.10−5.80; arithmetic mean, 4.95)[42,43] and plasma conditions, respectively. For compound (**3**), a decrease with time of the absorbance maximum at 410 nm along with an increase in the maximum at 317 nm, characteristic of pyridoxal, were observed both in citrate buffer pH = 5.0 and phosphate buffer pH = 7.4, suggesting the occurrence of hydrolyses, which is complete after 30 min (see Figures 7 and 8).

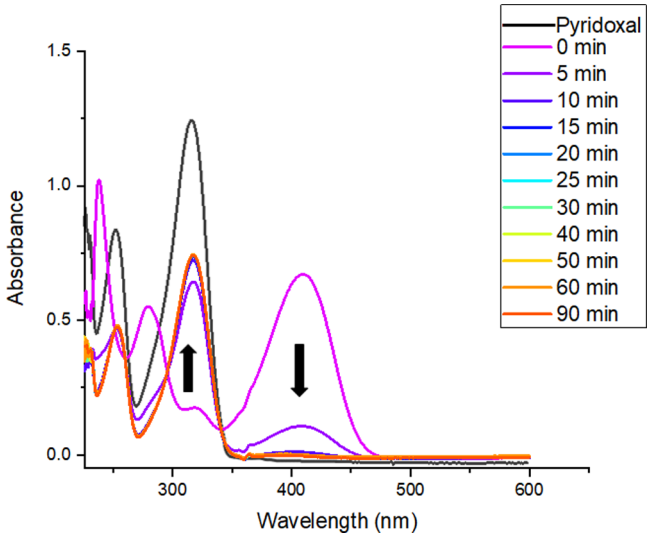

Figure 7. Time-dependent absorption spectra of compound (**3**) (5×10^{-5} mol·L^{-1}) in the citrate buffer (pH = 5.0).

Therefore, considering the lower hydration content of skin layers in comparison to the conditions employed in the current in vitro simulation, the results suggest that **3** would probably not be promptly hydrolyzed in a passive transdermal

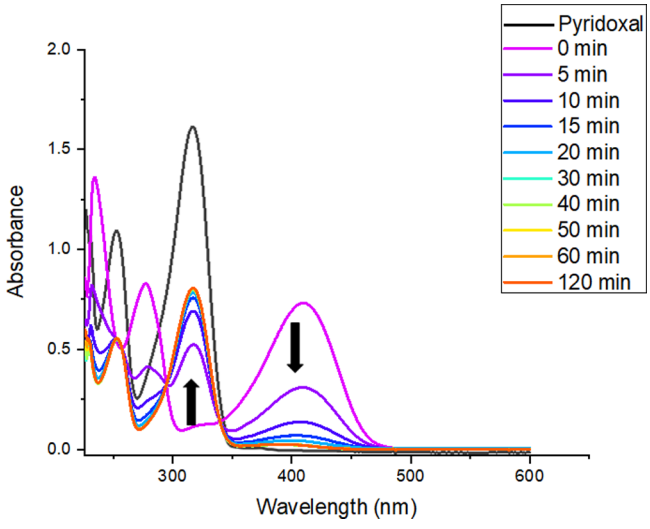

Figure 8. Time-dependent absorption spectra of compound (**3**) (5×10^{-5} mol·L^{-1}) in the phosphate buffer (pH = 7.4).

https://doi.org/10.1021/acsomega.1c06571
ACS Omega 2022, 7, 11678−11687

administration, allowing its delivery to adjacent tissues. In fact, the electronic spectra of **3** in dimethyl sulfoxide (DMSO) (see Figure S18) show increased stability of the compound in comparison to aqueous media.

Once in these tissues and eventually in the bloodstream, hydrolysis of **3** would be complete, avoiding the permanence of the intact Schiff base in the organism and its potential noncharacterized toxic effects. Hydrolysis of **3** results in the release of pyridoxal, a daily cofactor in human metabolism. Thus, from a toxicological profile perspective, **3** would also be the most promising compound.

CONCLUSIONS

Memantine-based prodrugs have been described in the literature, such as that obtained by replacing the memantine amino group with isothiocyanate as a putative H_2S donor. The compound showed an ability to release H_2S through a cysteine-mediated process, generating memantine.[44]

The design of prodrug candidates and carriers displaying proteolytically or hydrolytically cleavable C=N bonds has been previously explored for the release of the antitumor drug doxorubicin by a pH-sensitive hydrolysis.[45−50] In this context, Schiff base-derived conjugates have been described as promising cancer therapy alternatives according to their pH responsiveness.[51,52]

The new memantine−pyridoxal prodrug candidate reported in the present work might improve the transdermal administration of the NMDA antagonist. The resulting changes in drug physicochemical properties by this derivatization shed light on a therapeutically suitable approach especially important to AD patients with compromised swallowing.

Considering the challenges in the current pharmacotherapy administration, the outcomes described here pave the way for new proposals aiming at future alternatives for transdermal patches that might have applications in the treatment of neuropsychiatric conditions in general, such as Schizophrenia and related disorders,[53−55] which might increase treatment adherence, with life quality improvement of patients, families, and professional caregivers.

EXPERIMENTAL SECTION

Materials and General Procedures. All common chemicals were purchased from Aldrich and were used without further purification. The compounds were characterized by means of microanalyses, and their infrared, ^{1}H, ^{13}C, DEPT 135, correlation spectroscopy (COSY), HMQC, and HMBC NMR spectra. Elemental analyses were performed on a PerkinElmer CHN 2400 analyzer. Infrared (IR) spectra were recorded on a PerkinElmer FT-IR Spectrum GX spectrometer using KBr pellets (4000−400 cm^{-1}). NMR spectra were obtained with a Bruker DPX-400 ADVANCE (400 MHz) spectrometer using DMSO-d_6 as the solvent and tetramethylsilane as an internal reference. The ^{1}H resonances were assigned on the basis of chemical shifts, multiplicities, and by using 2D homonuclear ^{1}H−^{1}H COSY. The carbon type (C, CH) was determined by using distortionless enhancement by polarization transfer (DEPT-135) experiments, and the assignments were made by 2D heteronuclear multiple quantum coherence (HMQC) experiments.

Syntheses of Compounds (1−3). *2-[(E)-[(3,5-Dimethyladamantan-1-yl)imino]methyl]phenol (**1**).* Memantine hydrochloride (500 mg) was dissolved in water with the addition of NaOH until saturation. Upon liquid−liquid extraction in water/dichloromethane, **Me** was isolated in the organic phase. Compound (**1**) was obtained by mixing equimolar amounts (1 mmol) of **Me** with salicylaldehyde and triethylamine in dichloromethane. The reaction mixture was kept under reflux for 6 h followed by stirring at room temperature for 18 h. After reduction of the solvent by 90%, a solution of 1:1 hexane/diethyl ether was added, and the reaction mixture was kept in the refrigerator for 12 h. Afterward, the unreacted **Me** was filtered off, and the amber liquid was dried under reduced pressure. Anal. Calc. for $C_{19}H_{25}NO$ (FW = 283.41 g mol^{-1}): C, 80.52; H, 8.89; N, 4.94. Found: C, 80.59; H, 8.38; N, 4.96. IR (KBr, cm^{-1}): 1627 ν(C=N); 1280 ν(C−O). δ ^{1}H NMR [400.13 MHz, DMSO-d_6, δ(ppm)]: 14.35 (s, 1H, O−H) 8.56 (s, 1H, H13), 7.46 (dd, J = 7.6, 1.6 Hz, 1H, H15), 7.35−7.23 (t, 1H, H17), 6.89−6.79 (m, 2H, H16/18), 2.20 (dt, J = 6.1, 3.0 Hz, 1H, H7), 1.64 (d, J = 2.0 Hz, 2H, H8), 1.46−1.40 (m, 4H, H2/9), 1.40−1.32 (m, 4H, H6/10), 1.19 (s, 2H, H4), 0.89 (s, 6H, H11/12). δ ^{13}C{^{1}H} NMR [100,61 MHz, DMSO-d_6, δ(ppm)]: 161.5 (C19), 160.9 (C13), 132.1 (C17), 131.9 (C15), 118.7 (C14), 118.0/116.6 (C16/18), 58.5 (C1), 50.0 (C4), 48.5 (C2/9), 42.0 (C6/10), 41.0 (C8), 32.1 (C3/5), 30.0 (C11/12), 29.6 (C7). Yield: 45% (amber liquid).

*(E)-N-(3,5-Dimethyladamantan-1-yl)-1-(pyridin-2-yl) Methanimine (**2**).* Memantine (Me) was obtained from memantine hydrochloride as previously described. Compound (**2**) was obtained by mixing equimolar amounts (1 mmol) of **Me** and 2-pyridinecarboxaldehyde in dichloromethane. The reaction mixture was kept under reflux for 6 h, and the reaction was followed by thin-layer chromatography. After 24 h, the solvent was evaporated, and a solution of hexane/diethylether was added. Afterward, the reaction mixture was kept in the refrigerator for 12 h, and then the unreacted **Me** was filtered off, and the solvent was reduced by 90% in the dark. The resulting solid was filtered off, washed with diethylether, and dried under reduced pressure. Anal. Calc. for $C_{18}H_{24}N_2$ (FW = 268.40 g mol^{-1}): C, 80.55; H, 9.01; N, 10.44. Found: C, 80.15; H, 9.02; N, 10.29. Melting point: 43−45 °C. IR (KBr, cm^{-1}): 1644 ν(C=N). δ ^{1}H NMR [400.13 MHz, DMSO-d_6, δ(ppm)]: 8.62 (d, J = 4.7 Hz, 1H, H18), 8.27 (s, 1H, H13), 7.93 (d, J = 7.9 Hz, 1H, H15), 7.84 (t, J = 7.6 Hz, 1H, H16), 7.43 (dd, J = 6.5, 5.6 Hz, 1H, H17), 2.18 (s, 1H, H7), 1.60 (d, J = 1.6 Hz, 2H, H8), 1.41−1.37 (m, 4H, H2/9), 1.37−1.28 (m, 4H, H6/10), 1.17 (s, 2H, H4), 0.87 (s, 6H, H11/12). δ ^{13}C {^{1}H} NMR [100,61 MHz, DMSO-d_6, δ(ppm)]: 156.1 (C14), 155.0 (C13), 149.3 (C18), 136.8 (C16), 124.9 (C17), 120.0 (C15), 59.5 (C1), 50.3 (C4), 48.7 (C2/9), 42.3 (C6/10), 41.0 (C8), 32.1 (C3/5), 30.2 (C11/12), 29.7 (C7). Yield: 42% (amber solid).

*4-[(E)-[(3,5-Dimethyladamantan-1-yl)imino]methyl]-5-(hydroxymethyl)-2-methylpyridin-3-ol (**3**, **PyMe**).* Compound (**3**) was obtained by mixing 3 mmol of memantine hydrochloride with equimolar amounts of triethylamine and pyridoxaldehyde in 100 mL of dichloromethane under reflux. The reaction mixture was kept under stirring for 4 h. After cooling to room temperature, 200 mL of diethylether were added. The resulting precipitate was filtered off and washed with diethylether and dried under reduced pressure. Anal. Calc. For $C_{20}H_{28}N_2O_2$ (FW = 328.45 g mol^{-1}): C, 73.14; H, 8.59; N, 8.53. Found: C, 73.14; H, 8.64; N, 8.52. Melting point: 159.0−160.7 °C. IR (KBr, cm^{-1}): 3405/3263 ν(O−H), 1632 ν(C=N), 1399 ν(C−N), 650 ρ(py). δ ^{1}H NMR [400.13 MHz, DMSO-d_6, δ(ppm)]: 15.21 (s, 1H, O1−H), 8.82 (s, 1H,

https://doi.org/10.1021/acsomega.1c06571
ACS Omega 2022, 7, 11678−11687

H13), 7.82 (s, 1H, H16), 5.33 (s, 1H, O2−H), 4.65 (s, 2H, H21), 2.35 (s, 3H, H20), 2.22 (s, 1H, H7), 1.68 (s, 2H, H8), 1.52−1.32 (m, 8H, H2/6/9/10), 1.19 (s, 2H, H4), 0.89 (s, 6H, H11/12). $^{13}C\{^{1}H\}$ NMR [100.61 MHz, DMSO-d_6, δ(ppm)]: 158.5 (C13), 155.3 (C19), 148.8 (C18), 136.6 (C16), 132.8 (C14), 118.7 (C15), 59.4 (C1), 58.5 (C21), 49.9 (C4), 48.1 (C2/9), 41.9 (C6/10), 40.7 (C8), 32.1 (C3/5), 29.9 (C11/12), 29.5 (C7), 18.7 (C20). Yield: 84% (yellow solid).

Crystal Structure Determination. The single-crystal X-ray diffraction data for **2** and **3** were collected in an Oxford-Rigaku Gemini A Ultra diffractometer using MoKα (λ = 0.71073 Å) radiation at room temperature (298 K). The data collection, cell refinements, and data reduction were performed using the CRYSALISPRO software.[56] The structures were resolved by direct methods using SIR[57] and refined using the SHELXL-2018/3 program package.[58] All nonhydrogen atoms were refined with anisotropic thermal parameters. H atoms connected to carbon were placed in idealized positions and treated by a rigid model, with Uiso(H) = 1.2Ueq(C), and H atoms from NH groups were obtained directly by difference maps and also treated by a rigid model, with Uiso(H) = 1.2Ueq(N). The figures were drawn using ORTEP-3 for Windows[59] and Mercury.[60] The quantitative analyses of intermolecular interactions were made using the CrystalExplorer[61] program. CCDC 2100774 and 2100775 contain the supplementary crystallographic data for compounds (**2**) and (**3**), respectively.

Electronic Spectra. Electronic spectra were acquired with a Shimadzu UV-2401PC double beam UV−Vis spectrophotometer using 1 cm quartz cells. The spectra of 5% DMSO solutions of **3** (5×10^{-5} mol·L^{-1}) were recorded each for 5 min up to 90 min in citrate buffer pH = 5.0 and each 5 min up to 120 min in phosphate buffer pH = 7.4.

Speciation Prediction Studies. Speciation diagrams considering pH values between 0 and 14 and pKa, logP, and logD values were predicted for **1**, **2**, and **3** using the Chemicalize software.[20,21]

Solubility of Memantine Hydrochloride and 3 in N-octanol. Dansyl chloride was used for high-performance liquid chromatography (HPLC) derivatization, and *n*-octanol was purchased from Sigma-Aldrich (St. Louis, USA). The analyses were performed in an Agilent 1260 Infinity HPLC system (Agilent Technologies, CA, USA) equipped with a quaternary pump, an autosampler, a column oven, and a photodiode array detector. To compare the lipophilicity of memantine hydrochloride and **3**, excess amounts of both compounds were dispersed in 2 mL of *n*-octanol−∼150 mg of memantine hydrochloride and 300 mg of **3**. The supersaturated solutions were shaken at 150 rpm at 25 °C for 24 h. Afterward, the samples were centrifuged at 14 000 g for 15 min to remove the insoluble fractions. The supernatant was diluted first in phosphate-buffered saline buffer pH 7 followed by a dansylation reaction to allow the detection of derivatized memantine using HPLC[12] to determine the concentration of soluble compounds. Briefly, 100 μL of each solution was transferred to an Eppendorf tube, in which 100 μL of an alkaline buffer solution (pH 10.6) and 300 μL of a dansyl chloride solution (0.57 mg/mL in ACN) were added. The mixture was vortexed for 30 s and kept in the dark for 45 min at 50 °C. Afterward, the mixture was cooled in ice water for 10 min, and two phases were clearly formed. An aliquot of the upper layer containing the derivatized memantine was collected and injected into HPLC. The injection volume was 50 μL, and UV detection was performed at 218 nm. The separation was carried out on a Hypersil BDS-C18 column (150 × 4.6 mm, 5 μm), using a mixture of methanol/water (80:20) pH 3.0 as the mobile phase with a flow rate of 1.2 mL/min.

■ ASSOCIATED CONTENT

Supporting Information

The Supporting Information is available free of charge at https://pubs.acs.org/doi/10.1021/acsomega.1c06571.

Crystallographic information for compound **2** (CIF)

Crystallographic information for compound **3** (CIF)

NMR and infrared spectra of compounds (**1**−**3**), absorption spectra with time of compound (**3**) (5.0×10^{-5} mol·L^{-1}) in DMSO solution, speciation diagrams for **Me** and compounds (**1**−**2**), and selected bond distances and angles in the crystal structures of **2** and **3** (PDF)

■ AUTHOR INFORMATION

Corresponding Authors

Rafael P. Vieira − *Departamento de Bioquímica e Imunologia, Instituto de Ciências Biológicas, Universidade Federal de Minas Gerais, Belo Horizonte 31270-901 MG, Brazil*; Email: vieirarp@icb.ufmg.br

Heloisa Beraldo − *Departamento de Química, Instituto de Ciências Exatas, Universidade Federal de Minas Gerais, Belo Horizonte 31270-901 MG, Brazil*; orcid.org/0000-0001-8593-4555; Email: hberaldo@ufmg.br, heloisaberaldoufmg@gmail.com

Authors

Ana P. Araujo de Oliveira − *Departamento de Química, Instituto de Ciências Exatas, Universidade Federal de Minas Gerais, Belo Horizonte 31270-901 MG, Brazil*

Victoria C. Romero Colmenares − *Departamento de Química, Instituto de Ciências Exatas, Universidade Federal de Minas Gerais, Belo Horizonte 31270-901 MG, Brazil*

Renata Diniz − *Departamento de Química, Instituto de Ciências Exatas, Universidade Federal de Minas Gerais, Belo Horizonte 31270-901 MG, Brazil*

Jennifer T. J. Freitas − *Departamento de Química, Instituto de Ciências Exatas, Universidade Federal de Minas Gerais, Belo Horizonte 31270-901 MG, Brazil*

Clara M. da Cruz − *Departamento de Bioquímica e Imunologia, Instituto de Ciências Biológicas, Universidade Federal de Minas Gerais, Belo Horizonte 31270-901 MG, Brazil*

Eduardo B. Lages − *Departamento de Produtos Farmacêuticos, Faculdade de Farmácia, Universidade Federal de Minas Gerais, Belo Horizonte 31270-901 MG, Brazil*; orcid.org/0000-0002-2458-6021

Lucas A. M. Ferreira − *Departamento de Produtos Farmacêuticos, Faculdade de Farmácia, Universidade Federal de Minas Gerais, Belo Horizonte 31270-901 MG, Brazil*

Complete contact information is available at: https://pubs.acs.org/10.1021/acsomega.1c06571

Notes

The authors declare no competing financial interest.

https://doi.org/10.1021/acsomega.1c06571
ACS Omega 2022, 7, 11678−11687

■ ACKNOWLEDGMENTS

C.M.C. and R.P.V. thank PRPq-UFMG (ADRC 11/2017) and Fundação de Amparo à Pesquisa de Minas Gerais (FAPEMIG, APQ-01532-18). H.B. gratefully acknowledges CNPq (421902/2016-7, 305863/2018-5), CAPES, and FAPEMIG (APQ-00628-16) for the financial support and student grants.

■ REFERENCES

(1) WHO. Risk Reduction Of Cognitive Decline And Dementia https://www.ncbi.nlm.nih.gov/books/NBK542796/ (accessed Sep 26, 2021).
(2) Shankar, G. M.; Li, S.; Mehta, T. H.; Garcia-Munoz, A.; Shepardson, N. E.; Smith, I.; Brett, F. M.; Farrell, M. A.; Rowan, M. J.; Lemere, C. A.; Regan, C. M.; Walsh, D. M.; Sabatini, B. L.; Selkoe, D. J. Amyloid-β protein dimers isolated directly from Alzheimer's brains impair synaptic plasticity and memory. *Nat. Med.* **2008**, *14*, 837−842.
(3) Walsh, D. M.; Selkoe, D. J. Amyloid β-protein and beyond: the path forward in Alzheimer's disease. *Curr. Opin. Neurobiol.* **2020**, *61*, 116−124.
(4) Huang, X.; Atwood, C. S.; Hartshorn, M. A.; Multhaup, G.; Goldstein, L. E.; Scarpa, R. C.; Cuajungco, M. P.; Gray, D. N.; Lim, J.; Moir, R. D.; Tanzi, R. E.; Bush, A. I. The Aβ Peptide of Alzheimer's Disease Directly Produces Hydrogen Peroxide through Metal Ion Reduction. *Biochemistry* **1999**, *38*, 7609−7616.
(5) Adlard, P. A.; Bush, A. I. Metals and Alzheimer's Disease: How Far Have We Come in the Clinic? *J. Alzheimer's Dis.* **2018**, *62*, 1369−1379.
(6) Gomes, L. M. F.; Bataglioli, J. C.; Storr, T. Metal complexes that bind to the amyloid-β peptide of relevance to Alzheimer's disease. *Coord. Chem. Rev.* **2020**, *412*, 213255.
(7) Rossi, M.; Freschi, M.; De Camargo Nascente, L.; Salerno, A.; De Melo Viana Teixeira, S.; Nachon, F.; Chantegreil, F.; Soukup, O.; Prchal, L.; Malaguti, M.; Bergamini, C.; Bartolini, M.; Angeloni, C.; Hrelia, S.; Soares Romeiro, L. A.; Bolognesi, M. L. Sustainable Drug Discovery of Multi-Target-Directed Ligands for Alzheimer's Disease. *J. Med. Chem.* **2021**, *64*, 4972−4990.
(8) Mullard, A. Landmark Alzheimer's drug approval confounds research community. *Nature* **2021**, *594*, 309−310.
(9) Marotta, G.; Basagni, F.; Rosini, M.; Minarini, A. Memantine Derivatives as Multitarget Agents in Alzheimer's Disease. *Molecules* **2020**, *25*, 4005.
(10) Calhoun, A.; King, C.; Khoury, R.; Grossberg, G. T. An evaluation of memantine ER + donepezil for the treatment of Alzheimer's disease. *Expert Opin. Pharmacother.* **2018**, *19*, 1711−1717.
(11) Sevilla, C.; Jiménez Caballero, P. E.; Alfonso, V.; González-Adalid, M. Current Treatments of Alzheimer Disease: Are Main Caregivers Satisfied with the Drug Treatments Received by Their Patients? *Dementia Geriatr. Cognit. Disord.* **2009**, *28*, 196−205.
(12) Del Rio-Sancho, S.; Serna-Jiménez, C. E.; Calatayud-Pascual, M. A.; Balaguer-Fernández, C.; Femenía-Font, A.; Merino, V.; López-Castellano, A. Transdermal Absorption of Memantine - Effect of Chemical Enhancers, Iontophoresis, and Role of Enhancer Lipophilicity. *Eur. J. Pharm. Biopharm.* **2012**, *82*, 164−170.
(13) Di Stefano, A.; Sozio, P.; Cerasa, L. S.; Marinelli, L. Transdermal donepezil on the treatment of Alzheimer's disease. *Neuropsychiatr. Dis. Treat.* **2012**, *8*, 361.
(14) Adler, G.; Mueller, B.; Articus, K. The transdermal formulation of rivastigmine improves caregiver burden and treatment adherence of patients with Alzheimer's disease under daily practice conditions. *Int. J. Clin. Pract.* **2014**, *68*, 465−470.
(15) Gomes, L. M. F.; Vieira, R. P.; Jones, M. R.; Wang, M. C. P.; Dyrager, C.; Souza-Fagundes, E. M.; Da Silva, J. G.; Storr, T.; Beraldo, H. 8-Hydroxyquinoline Schiff-base compounds as antioxidants and modulators of copper-mediated Aβ peptide aggregation. *J. Inorg. Biochem.* **2014**, *139*, 106−116.
(16) Vieira, R. P.; Thompson, J. R.; Beraldo, H.; Storr, T. Partial conversion of thioamide into nitrile in a copper(II) complex of 2,6-diacetylpyridine bis(thiosemicarbazone), a drug prototype for Alzheimer's disease. *Acta Crystallogr., Sect. C: Struct. Chem.* **2015**, *71*, 430−434.
(17) Bruno, I. J.; Cole, J. C.; Kessler, M.; Luo, J.; Motherwell, W. D. S.; Purkis, L. H.; Smith, B. R.; Taylor, R.; Cooper, R. I.; Harris, S. E.; Orpen, A. G. Retrieval of Crystallographically-Derived Molecular Geometry Information. *J. Chem. Inf. Comput. Sci.* **2004**, *44*, 2133−2144.
(18) Spackman, M. A.; Jayatilaka, D. Hirshfeld Surface Analysis. *CrystEngComm* **2009**, *11*, 19−32.
(19) Spackman, M. A.; McKinnon, J. J. Fingerprinting Intermolecular Interactions in Molecular Crystals. *CrystEngComm* **2002**, *4*, 378−392.
(20) Copyright © 1998-2019 ChemAxon Ltd., C.-I. C. S. Chemicalize https://chemicalize.com/app/calculation (accessed June 18, 2021).
(21) Swain, M. chemicalize.org. *J. Chem. Inf. Model.* **2012**, *52*, 613−615.
(22) Brown, M. B.; Martin, G. P.; Jones, S. A.; Akomeah, F. K. Dermal and Transdermal Drug Delivery Systems: Current and Future Prospects. *Drug Delivery* **2006**, *13*, 175−187.
(23) Bos, J. D.; Meinardi, M. M. H. M. The 500 Dalton Rule for the Skin Penetration of Chemical Compounds and Drugs. *Exp. Dermatol.* **2000**, *9*, 165−169.
(24) Pastore, M. N.; Kalia, Y. N.; Horstmann, M.; Roberts, M. S. Transdermal Patches: History, Development and Pharmacology. *Br. J. Pharmacol.* **2015**, *172*, 2179−2209.
(25) Yano, T.; Nakagawa, A.; Tsuji, M.; Noda, K. Skin Permeability of Various Non-Steroidal Anti-Inflammatory Drugs in Man. *Life Sci.* **1986**, *39*, 1043−1050.
(26) IUPAC - Schiff bases (S05498) https://goldbook.iupac.org/terms/view/S05498 (accessed Oct 1, 2021).
(27) IUPAC - aldimines (A00209) https://goldbook.iupac.org/terms/view/A00209 (accessed Oct 1, 2021).
(28) IUPAC - ketimines (K03381) https://goldbook.iupac.org/terms/view/K03381 (accessed Oct 1, 2021).
(29) Vieira, R. P.; Lessa, J. A.; Ferreira, W. C.; Costa, F. B.; Bastos, L. F. S.; Rocha, W. R.; Coelho, M. M.; Beraldo, H. Influence of Susceptibility to Hydrolysis and Hydrophobicity of Arylsemicarbazones on Their Anti-Nociceptive and Anti-Inflammatory Activities. *Eur. J. Med. Chem.* **2012**, *50*, 140−148.
(30) Cordes, E. H.; Jencks, W. P. The Mechanism of Hydrolysis of Schiff Bases Derived from Aliphatic Amines. *J. Am. Chem. Soc.* **1963**, *85*, 2843−2848.
(31) Donoso, J.; Muñoz, F.; García Del Vado, A.; Echevarría, G.; García Blanco, F. Study of the hydrolysis and ionization constants of Schiff base from pyridoxal 5′-phosphate and n-hexylamine in partially aqueous solvents. An application to phosphorylase b. *Biochem. J.* **1986**, *238*, 137−144.
(32) Fahel, J. S.; Vieira, R. P.; Marinho, F. V.; Santos, V. C.; de Assis, J. V.; Corsetti, P. P.; Ferreira, R. S.; de Almeida, M. V.; Oliveira, S. C. JVA, an Isoniazid Analogue, Is a Bioactive Compound against a Clinical Isolate of the Mycobacterium Avium Complex. *Tuberculosis* **2019**, *115*, 108−112.
(33) Raboni, S.; Spyrakis, F.; Campanini, B.; Amadasi, A.; Bettati, S.; Peracchi, A.; Mozzarelli, A.; Contestabile, R. Pyridoxal 5′-Phosphate-Dependent Enzymes: Catalysis, Conformation, and Genomics. *Compr. Nat. Prod. II Chem. Biol.* **2010**, *7*, 273−350.
(34) Kirsch, J. F.; Eichele, G.; Ford, G. C.; Vincent, M. G.; Jansonius, J. N.; Gehring, H.; Christen, P. Mechanism of Action of Aspartate Aminotransferase Proposed on the Basis of Its Spatial Structure. *J. Mol. Biol.* **1984**, *174*, 497−525.
(35) Kochhar, S.; Christen, P. Mechanism of Racemization of Amino Acids by Aspartate Aminotransferase. *Eur. J. Biochem.* **1992**, *203*, 563−569.
(36) Cubellis, M. V.; Rozzo, C.; Nitti, G.; Arnone, M. I.; Marino, G.; Sannia, G. Cloning and Sequencing of the Gene Coding for Aspartate Aminotransferase from the Thermoacidophilic Archaebacterium Sulfolobus Solfataricus. *Eur. J. Biochem.* **1989**, *186*, 375−381.

https://doi.org/10.1021/acsomega.1c06571
ACS Omega 2022, 7, 11678−11687

(37) Johnstone, D. L.; Al-Shekaili, H. H.; Tarailo-Graovac, M.; Wolf, N. I.; Ivy, A. S.; Demarest, S.; Roussel, Y.; Ciapaite, J.; Van Roermund, C. W. T.; Kernohan, K. D.; Kosuta, C.; Ban, K.; Ito, Y.; McBride, S.; Al-Thihli, K.; Abdelrahim, R. A.; Koul, R.; Al Futaisi, A.; Haaxma, C. A.; Olson, H.; Sigurdardottir, L. Y.; Arnold, G. L.; Gerkes, E. H.; Boon, M.; Heiner-Fokkema, M. R.; Noble, S.; Bosma, M.; Jans, J.; Koolen, D. A.; Kamsteeg, E.-J.; Drögemöller, B.; Ross, C. J.; Majewski, J.; Cho, M. T.; Begtrup, A.; Wasserman, W. W.; Bui, T.; Brimble, E.; Violante, S.; Houten, S. M.; Wevers, R. A.; Van Faassen, M.; Kema, I. P.; Lepage, N.; Lines, M. A.; Dyment, D. A.; Wanders, R. J. A.; Verhoeven-Duif, N.; Ekker, M.; Boycott, K. M.; Friedman, J. M.; Pena, I. A.; Van Karnebeek, C. D. M. PLPHP Deficiency: Clinical, Genetic, Biochemical, and Mechanistic Insights. *Brain* **2019**, *142*, 542−559.
(38) Wilson, M. P.; Plecko, B.; Mills, P. B.; Clayton, P. T. Disorders affecting vitamin B 6 metabolism. *J. Inherited Metab. Dis.* **2019**, *42*, 629−646.
(39) van Kessel, S. P.; Frye, A. K.; El-Gendy, A. O.; Castejon, M.; Keshavarzian, A.; van Dijk, G.; El Aidy, S. Gut bacterial tyrosine decarboxylases restrict levels of levodopa in the treatment of Parkinson's disease. *Nat. Commun.* **2019**, *10*, 310.
(40) Rekdal, V. M.; Bess, E. N.; Bisanz, J. E.; Turnbaugh, P. J.; Balskus, E. P. Discovery and Inhibition of an Interspecies Gut Bacterial Pathway for Levodopa Metabolism. *Science* **2019**, *364*, No. eaau6323.
(41) Eliot, A. C.; Kirsch, J. F. Pyridoxal Phosphate Enzymes: Mechanistic, Structural, and Evolutionary Considerations. *Annu. Rev. Biochem.* **2004**, *73*, 383−415.
(42) Proksch, E. pH in Nature, Humans and Skin. *J. Dermatol.* **2018**, *45*, 1044−1052.
(43) Segger, D.; Aßmus, U.; Brock, M.; Erasmy, J.; Finkel, P.; Fitzner, A.; Heuss, H.; Kortemeier, U.; Munke, S.; Rheinländer, T.; Schmidt-Lewerkühne, H.; Schneider, W.; Weser, G. Multicenter Study on Measurement of the Natural pH of the Skin Surface. *Int. J. Cosmet. Sci.* **2008**, *30*, 75.
(44) Sestito, S.; Daniele, S.; Pietrobono, D.; Citi, V.; Bellusci, L.; Chiellini, G.; Calderone, V.; Martini, C.; Rapposelli, S. Memantine Prodrug as a New Agent for Alzheimer's Disease. *Sci. Rep.* **2019**, *9*, 4612.
(45) Du, J.-Z.; Du, X.-J.; Mao, C.-Q.; Wang, J. Tailor-Made Dual PH-Sensitive Polymer-Doxorubicin Nanoparticles for Efficient Anticancer Drug Delivery. *J. Am. Chem. Soc.* **2011**, *133*, 17560−17563.
(46) Etrych, T.; Šubr, V.; Laga, R.; Říhová, B.; Ulbrich, K. Polymer Conjugates of Doxorubicin Bound through an Amide and Hydrazone Bond: Impact of the Carrier Structure onto Synergistic Action in the Treatment of Solid Tumours. *Eur. J. Pharm. Sci.* **2014**, *58*, 1−12.
(47) Říhová, B.; Etrych, T.; Pechar, M.; Jelínková, M.; Šťastný, M.; Hovorka, O.; Kovář, M.; Ulbrich, K. Doxorubicin Bound to a HPMA Copolymer Carrier through Hydrazone Bond Is Effective Also in a Cancer Cell Line with a Limited Content of Lysosomes. *J. Controlled Release* **2001**, *74*, 225−232.
(48) Seymour, L.; Ulbrich, K.; Steyger, P.; Brereton, M.; Subr, V.; Strohalm, J.; Duncan, R. Tumour Tropism and Anti-Cancer Efficacy of Polymer-Based Doxorubicin Prodrugs in the Treatment of Subcutaneous Murine B16F10 Melanoma. *Br. J. Cancer* **1994**, *70*, 636−641.
(49) Seymour, L. W.; Ulbrich, K.; Strohalm, J.; Kopeček, J.; Duncan, R. The Pharmacokinetics of Polymer-Bound Adriamycin. *Biochem. Pharmacol.* **1990**, *39*, 1125−1131.
(50) Říhová, B.; Etrych, T.; Šiérovaé, M.; Kovaéř, L.; Hovorka, O.; Kovaéř, M.; Benda, A.; Ulbrich, K. Synergistic Action of Doxorubicin Bound to the Polymeric Carrier Based on N-(2-Hydroxypropyl)-Methacrylamide Copolymers through an Amide or Hydrazone Bond. *Mol. Pharm.* **2010**, *7*, 1027−1040.
(51) Sonawane, S. J.; Kalhapure, R. S.; Govender, T. Hydrazone Linkages in pH Responsive Drug Delivery Systems. *Eur. J. Pharm. Sci.* **2017**, *99*, 45−65.
(52) Zhai, Y.; Zhou, X.; Zhang, Z.; Zhang, L.; Wang, D.; Wang, X.; Sun, W. Design, Synthesis, and Characterization of Schiff Base Bond-Linked pH-Responsive Doxorubicin Prodrug Based on Functionalized mPEG-PCL for Targeted Cancer Therapy. *Polymers* **2018**, *10*, 1127.
(53) Abruzzo, A.; Cerchiara, T.; Luppi, B.; Bigucci, F. Transdermal Delivery of Antipsychotics: Rationale and Current Status. *CNS Drugs* **2019**, *33*, 849−865.
(54) Suzuki, K.; Castelli, M.; Komaroff, M.; Starling, B.; Terahara, T.; Citrome, L. Pharmacokinetic Profile of the Asenapine Transdermal System (HP-3070). *J. Clin. Psychopharmacol.* **2021**, *41*, 286−294.
(55) Carrithers, B.; El-Mallakh, R. S. Transdermal Asenapine in Schizophrenia: A Systematic Review. *Patient Prefer. Adherence* **2020**, *Volume 14*, 1541−1551.
(56) Rigaku Oxford Diffraction. *CrysAlis Pro*; Rigaku Corporation: Tokyo, Japan, 2015.
(57) Burla, M. C.; Caliandro, R.; Carrozzini, B.; Cascarano, G. L.; Cuocci, C.; Giacovazzo, C.; Mallamo, M.; Mazzone, A.; Polidori, G. Crystal structure determination and refinementviaSIR2014. *J. Appl. Crystallogr.* **2015**, *48*, 306−309.
(58) Sheldrick, G. M. Crystal structure refinement withSHELXL. *Acta Crystallogr., Sect. C: Struct. Chem.* **2015**, *71*, 3−8.
(59) Farrugia, L. J. ORTEP-3 for Windows - a version ofORTEP-III with a Graphical User Interface (GUI). *J. Appl. Crystallogr.* **1997**, *30*, 565.
(60) Macrae, C. F.; Bruno, I. J.; Chisholm, J. A.; Edgington, P. R.; McCabe, P.; Pidcock, E.; Rodriguez-Monge, L.; Taylor, R.; Van De Streek, J.; Wood, P. A. Mercury CSD 2.0- new features for the visualization and investigation of crystal structures. *J. Appl. Crystallogr.* **2008**, *41*, 466−470.
(61) Spackman, P. R.; Turner, M. J.; McKinnon, J. J.; Wolff, S. K.; Grimwood, D. J.; Jayatilaka, D.; Spackman, M. A. CrystalExplorer: a program for Hirshfeld surface analysis, visualization and quantitative analysis of molecular crystals. *J. Appl. Crystalogr.* **2021**, *54*, 1006−1011.

https://doi.org/10.1021/acsomega.1c06571
ACS Omega 2022, 7, 11678−11687